Available online at www.sciencedirect.com
ScienceDirect
Trans. Nonferrous Met. Soc. China 31(2021) 565−575
Transactions of Nonferrous Metals Society of China
www.tnmsc.cn

Effect of casting speed on floating grains and macrosegregation of direct-chill cast 2024 alloy with intensive melt shearing

Xu-dong LIU[1,2], Qing-feng ZHU[1,2], Zhi-meng LI[1,2], Cheng ZHU[1,2], Rui WANG[1,2], Tao JIA[2,3], Zhi-hao ZHAO[2], Jian-zhong CUI[1,2], Yu-bo ZUO[1,2]

1. Key Lab of Electromagnetic Processing of Materials, Ministry of Education, Northeastern University, Shenyang 110004, China;
2. College of Materials Science and Engineering, Northeastern University, Shenyang 110004, China;
3. State Key Laboratory of Rolling and Automation, Northeastern University, Shenyang 110004, China

Received 4 May 2020; accepted 30 December 2020

Abstract: The ingot was prepared by direct-chill (DC) casting technology with different casting speeds under the influence of intensive melt shearing to explore the effect of casting speed and intensive melt shearing on the floating grains and negative centerline segregation. The results indicate that the application of intensive melt shearing in DC casting process can distribute the floating grains uniformly, reduce the area fraction of the floating grains, alleviate the negative centerline segregation, and improve the uniformity of temperature field in the sump. It is also suggested that under the influence of intensive melt shearing, the casting speed plays a crucial role in the amounts and distribution of floating grains. At low casting speed, the intensive melt shearing can significantly reduce the area fraction of the floating grains and distribute them uniformly throughout the ingot. However, this effect gradually disappears with the increase of casting speed.

Key words: direct-chill casting; intensive melt shearing; macrosegregation; floating grains; casting speed; 2024 aluminum alloy

1 Introduction

Direct-chill (DC) casting has been the major way to produce the wrought aluminum alloy ingots due to its easy-operation and high production efficiency. The defect-free as-cast structure is desirable for the DC cast ingots, which is conducive to improve the formability of the downstream deformation products and enhance the overall performance of the end products [1−4]. During the DC casting process, the melt first solidifies to form a solid shell under the primary cooling of the crystallizer. The solid shell then leaves the crystallizer as a consequence of the thermal contraction, forming an air gap. The heat transfer between the melt and the crystallizer decreases dramatically in the air gap zone, which could lead to partial remelting of the solid shell. The inner part of the ingot solidifies under the secondary cooling water, and the cooling rate gradually decreases from the surface to the center [5−8]. This makes it common that there are some defects such as inhomogeneous as-cast structure and severe macro-segregation in DC cast ingots, especially when casting large size ingots [9−11]. More importantly, inhomogeneous as-cast structure and macrosegregation cannot be eliminated during subsequent heat treatment [12−14]. As a consequence, it is necessary to control these casting defects during the DC casting process. Adjusting the casting parameters (such as casting speed, casting

Corresponding author: Yu-bo ZUO; Tel: +86-13904019603; E-mail: zuoyubo@epm.neu.edu.cn
DOI: 10.1016/S1003-6326(21)65519-X

temperature, and cooling water conditions) and applying an external field (such as electromagnetic stirring, mechanical stirring, and ultrasound) are common approaches to reduce these casting defects [15−18].

In the DC casting process, casting speed is a key parameter, which directly affects the formability, the distribution of floating grains, and the macrosegregation. In general, increasing the casting speed can somehow refine the grains and improve the production efficiency [19,20]. Meanwhile, higher casting speed will also increase the depth of the sump, resulting in macrosegregation aggravation [15,21,22].

Recently, FAN and his colleagues [23−26] have proposed intensive melt shearing and applied this technique in the DC casting process to refine grain and alleviate macrosegregation by affecting temperature field and flow field. In the casting process, the high-shear unit was inserted in the molten melt in the crystallizer. A forced convection is formed while avoiding the whirlpool and the violent fluctuation of the melt surface, as the video shown by LIU et al [27]. LI et al [25] reported that intensive melt shearing could lessen the percentage of microporosity while refining grains. WALINJKAR and RAO [28] have proven through simulation that the temperature field of the DC casting process can be uniform by using the stator−rotor high-shear unit to treat the melt. PATEL et al [29] demonstrated experimentally that the sump depth can be reduced by applying intensive melt shearing. In our recent work, we found that with the mixture of solid and liquid passing through the stator−rotor high-shear unit during DC casting process, the grain refining effect achieved by the intensive melt shearing was significantly improved [30].

For the intensive melt shearing technology, an optimal casting speed determined by both ingot quality and production efficiency is required in its industrial application. Although many valuable results about the intensive melt shearing on microstructure and macrosegregation have been obtained, there are few literatures on the effect of casting speed under the intensive melt shearing. In this work, we focus on the effect of casting speed on the floating grains and macrosegregation in DC cast 2024 alloy ingot with intensive melt shearing.

2 Experimental

Figure 1 shows the experimental facility used in this study, which mainly consists of an aluminum melting electric furnace, a crystallizer, a semi-continuous casting system, and a high-shear system. The inner wall of the crystallizer is embedded with a graphite ring with a height of 40 mm. The aluminum melt in the electric furnace enters the crystallizer through a launder. The high-shear system includes a stator−rotor unit made of graphite, a drive shaft, a motor, and the motor speed control device.

The 2024 aluminum alloy was used in the present work with the composition (wt.%) of 4.09 Cu, 1.51 Mg and 0.34 Mn. First, in an electric furnace, the pure aluminum was melted. Then, the pure copper was appended when the melted aluminum was at 740 °C. When the copper was completely melted and the temperature of the melt

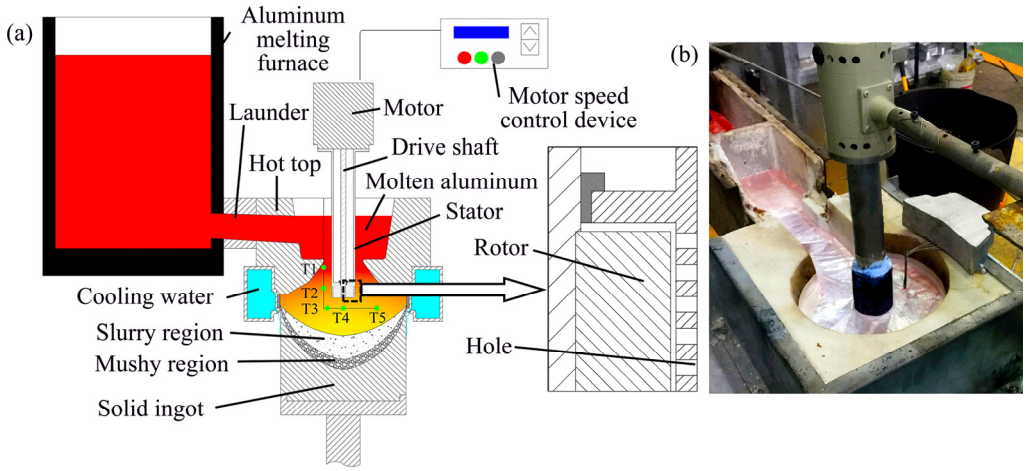

Fig. 1 Schematic of casting process and temperature measurement (a) and photo of DC casting process (b)

rose to 740 °C, Al−10Mn master alloy, and pure magnesium were added into the melt by a cover. After degassing with C2Cl6 and dross removing, the melt in the furnace was kept at 730 °C for 20 min, and then the stopper−rod was opened and the melt was introduced to the crystallizer through the launder. When the melt filled the cavity of the crystallizer, the cooling water was switched on and then the casting machine was started. The flow rate of cooling water was maintained at 150 L/min during the casting process.

At beginning, about 500 mm-long ingot was cast at the casting speed of 65 mm/min by the conventional DC casting technology. Then, the high-shear unit preheated to about 700 °C was inserted into the melt along the centerline of the crystallizer. The tip of the high-shear unit is 200 mm below the melt surface and 20 mm above the bottom of the graphite ring of the crystallizer. The rotational speed of the motor was set to be 3000 r/min. The casting speed was enhanced to be 75 mm/min when approximately 350 mm of the ingot was produced. After another 350 mm was cast, the casting speed was further risen to be 85 mm/min. The left part of the ingot was then cast at this speed.

To study the variation of temperature distribution under different casting conditions, five K-type thermocouples fixed on the stainless rod were used to record the temperatures. Thermocouples T3, T4 and T5 were placed on a plane 220 mm below the melt surface. Thermocouple T4 was placed in the center of the crystallizer. The distances between thermocouples T5 and T4, T3 and T4 are 100 and 50 mm, respectively. Thermocouples T1 and T2 were 70 mm away from the centerline of the ingot, and were 120 and 170 mm below the melt surface, respectively. All these thermocouples were linked to a data logger and the temperatures were recorded every 0.1 s.

All samples used for as-cast structure observation were cut from the center plane of the ingot. For microstructure observation, samples were taken at different locations in the radial direction of the ingot, as shown in Fig. 2. The dendrite microstructure was observed by etching with 5 wt.% HF aqueous solution. The grain size was studied by anodizing with HBF4 aqueous solution at a direct current voltage of 20 V. The grain size and the secondary dendrite arm spacing were measured using random line intercept technique.

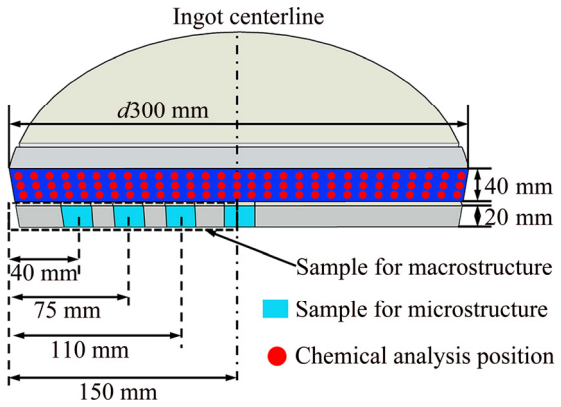

Fig. 2 Scheme of samples for as-cast structure observation and chemical analysis

A spectromax (Foundry master pro) was used to measure the composition of the ingot. The composition measurement was performed every 10 mm along the diameter (Fig. 2) and the average of the three tests was obtained as the result. The chemical composition near the surface of the ingot was also analyzed by processing the surface with a planer and spark spectrum testing. The degree of macrosegregation was characterized by ΔC (relative deviation):

$$\Delta C=(C_i-C_0)/C_0$$

where C_i is the average composition at a test location, and C_0 is the average composition of alloy.

3 Results

3.1 Temperature distribution

The temperature−time curves of different temperature measuring points are shown in Fig. 3. The melt temperature at each measurement point decreases rapidly and the temperature distribution becomes more uniform with the introduction of intensive melt shearing. In the conventional DC casting process, at the casting speed of 65 mm/min, the average temperature of the measurement points from T1 to T5 are 706, 703, 677, 683 and 673 °C, respectively. These temperatures are all above 642 °C (liquidus temperature of the experimental aluminum alloy). The temperature difference among the three measurement points (T3, T4 and T5) in the radial range of 100 mm and between the two measurement points (T1 and T2) in the axial range of 50 mm are 10 and 3 °C, respectively. After the high-shear unit was inserted and switched on,

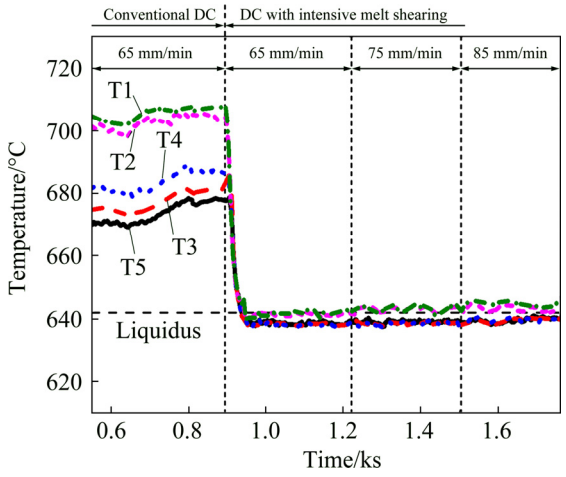

Fig. 3 Measured temperature−time curves during casting process

the average temperature of the measurement points from T1 to T5 are 642, 641, 638, 638 and 639 °C, respectively, which are much lower than the temperatures measured in conventional DC casting process. Statistical results also show that under the influence of intensive melt shearing, the temperature difference among the measurement points becomes much less. The difference of temperature among the three measurement points (T3, T4, and T5) in the radial range of 100 mm and between the two measurement points (T1 and T2) in the axial range of 50 mm are both 1 °C, indicating a more uniform temperature distribution in the casting process. In addition, it can be found that the melt temperature at T4 (center) is slightly lower than that at T3 (50 mm from the center) and T5 (100 mm from the center). This may be caused by the convection flow generated by the high-shear unit (at the center, melt flows from the lower part to the upper part until it is sucked into the high-shear unit). With casting speed increasing from 65 to 75 mm/min, the average temperatures of T1−T5 increase slightly to 643, 643, 639, 639 and 639 °C, respectively. Temperature difference among the three measurement points (T3, T4, and T5) in the radial direction and between the two measurement points (T1 and T2) in the axial direction are both 0 °C, which indicates that the uniformity of temperature distribution increases. After increasing the casting speed to 85 mm/min, the average temperatures of T1−T5 further increase to 645, 644, 640, 639 and 640 °C, respectively. The temperature difference among the three measurement points (T3, T4, and T5) in the radial direction and between the two measurement points (T1 and T2) in the axial direction are both 1 °C. The temperature distribution in the radial direction and the axial direction remains uniform.

3.2 As-cast structure

Figures 4 and 5 show the macrostructure and microstructure under polarized light of the ingot cast by DC casting technology and with different casting speeds under the influence of intensive melt shearing. For the conventional DC cast ingot, there are mainly feathery grains in the ingot edge. In the ingot center, there are equiaxed grains and the grain size is large. After the high-shear unit is inserted and switched on, the feathery grains disappear and the grain size becomes smaller, which indicates that the uniformity of the microstructure is enhanced. The grain morphology and the grain size do not change significantly with the increase of casting speed under intensive melt shearing. The distribution of grain size in the radial direction is shown in Fig. 6.

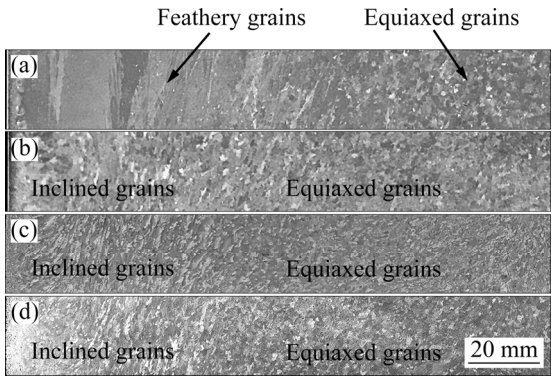

Fig. 4 Macrostructures of ingot produced under different casting conditions: (a) Conventional DC, 65 mm/min; (b) With shearing, 65 mm/min; (c) With shearing, 75 mm/min; (d) With shearing, 85 mm/min

The dendrite microstructure was examined to investigate the effect of casting speed on the floating grains in DC cast with intensive melt shearing, as shown in Fig. 7. For the conventional DC cast ingot, the floating grains (duplex structure composed of both coarse dendrite arms and fine dendrite arms, as marked by arrows) appear in the center of the ingot (Fig. 7(a)). The secondary dendrite arm spacing (SDAS) of the floating grains in the ingot center is given in Table 1. Under the influence of intensive melt shearing, the dendrite

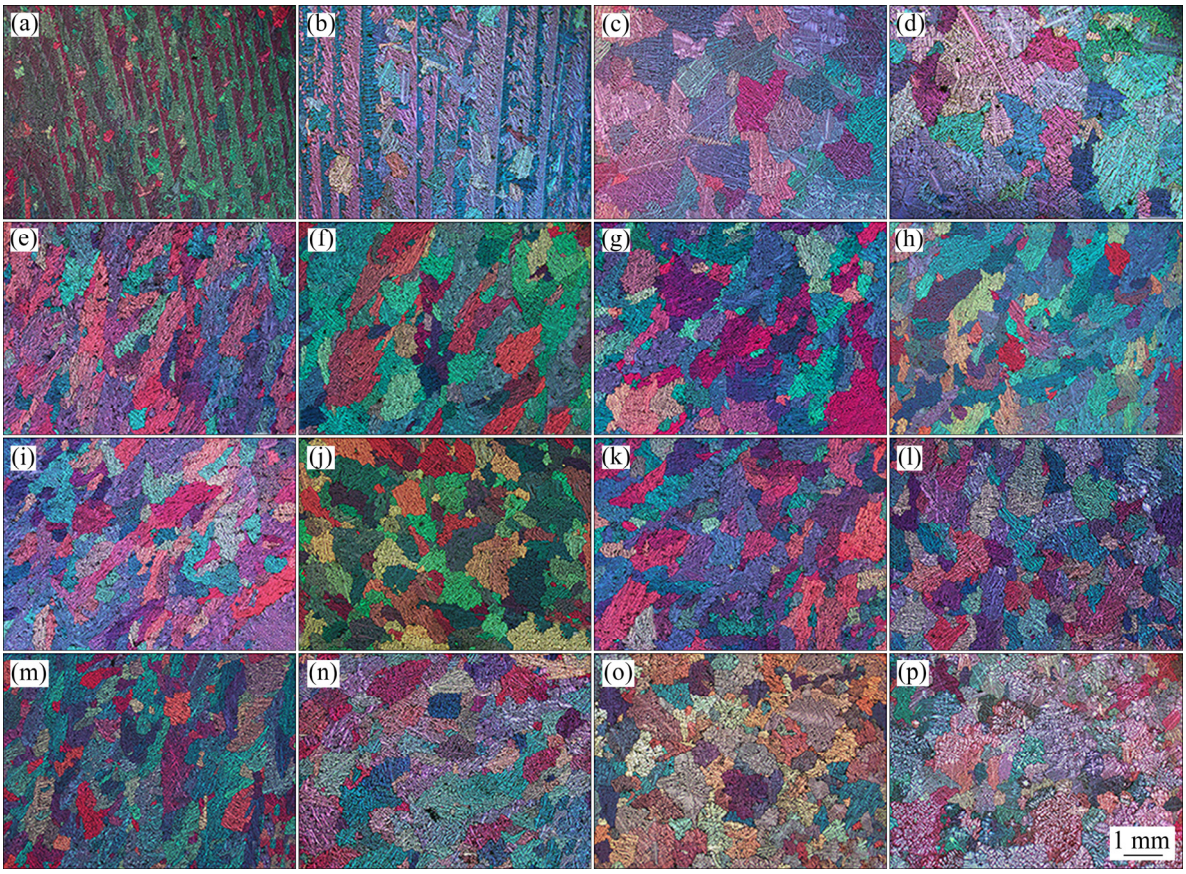

Fig. 5 Microstructures of ingot produced under different casting conditions: (a−d) Conventional DC, 65 mm/min; (e−h) With shearing, 65 mm/min; (i−l) With shearing, 75 mm/min; (m−p) With shearing, 85 mm/min; (a, e, i, m) 40 mm from surface; (b, f, j, n) 75 mm from surface; (c, g, k, o) 110 mm from surface; (d, h, l, p) Center

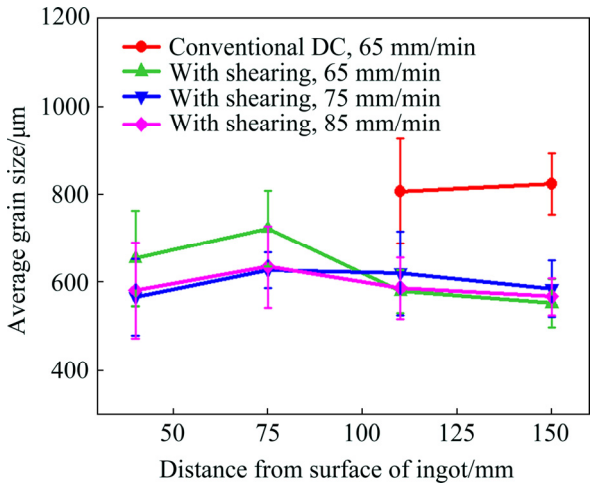

Fig. 6 Grain size distribution along radius (Note: grain size of the feathery grain is not counted)

arms are relatively small and uniform and the floating grains (coarse dendrite arms) almost disappear (Fig. 7(b)). With increasing casting speed to 75 mm/min under intensive melt shearing, there is a small amount of coarse dendrite arms in the center of the ingot and the area fraction of floating grains increases slightly (Fig. 7(c)). As the casting speed is further increased to 85 mm/min, the area fraction of floating grains in the ingot center increases significantly (Fig. 7(d)). The distribution of the floating grain in the radial direction of the ingot is shown in Fig. 8. It can be found that in the conventional DC cast ingot, there are many floating grains and the area fraction of floating grains increases from the surface to the center. When the high-shear unit is inserted and switched on at low casting speeds (65 and 75 mm/min), not only the area fraction of floating grain decreases sharply, but also the distribution is more uniform. However, as the casting speed is increased to 85 mm/min, the floating grains in the center region of the ingot increase significantly and the uniformity of distribution along the radius decreases.

To more intuitively reveal the transformation of the as-cast structure, the transition section of the ingot was selected and cut along the longitudinal section, and then its macrostructure was observed, as shown in Fig. 9. It can be seen that under the

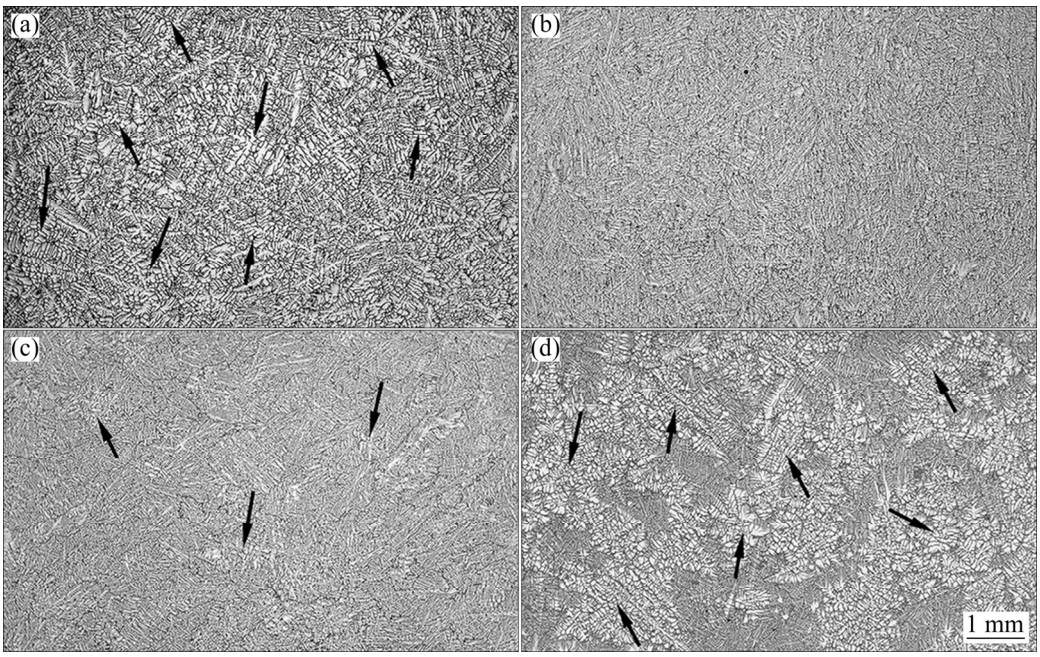

Fig. 7 Dendrite microstructures in ingot center: (a) Conventional DC, 65 mm/min; (b) With shearing, 65 mm/min; (c) With shearing, 75 mm/min; (d) With shearing, 85 mm/min

Table 1 SDAS of floating grains in ingot center (μm)

Grain	Conventional DC, 65 mm/min	With shearing, 65 mm/min	With shearing, 75 mm/min	With shearing, 85 mm/min
Coarse	60±5	–	48±4	56±6
Fine	26±3	26±3	24±2	22±2

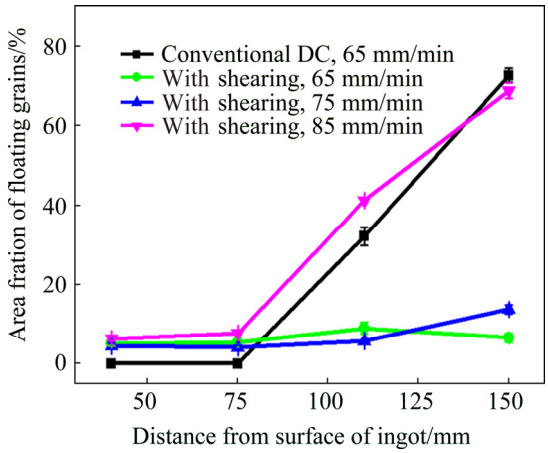

Fig. 8 Area fraction of floating grains along radius

influence of intensive melt shearing, floating grains transform into equiaxed grains with fine and uniform dendrite arms. This indicates that the area fraction of floating grains can be effectively reduced through intensive melt shearing.

3.3 Macrosegregation

The distribution of the ΔC of the Cu element along the diameter is shown in Fig. 10(a). In the subsurface and the center, there is serious negative segregation, while there is obvious positive segregation on the surface. For the conventional DC cast ingot, the ΔC values of the Cu element on the surface, in the subsurface and in the center are 0.776, −0.159 and −0.094, respectively. After the high-shear unit was inserted and switched on, the ΔC on the surface and in the subsurface in absolute is still large, while the negative centerline segregation is significantly reduced to −0.042. Under the influence of intensive melt shearing, as the casting speed increases, the negative centerline segregation becomes more serious. At the casting speeds of 75 and 85 mm/min, the ΔC values in the center are −0.065 and −0.084, respectively.

Figure 10(b) shows the distribution of the ΔC of the Mg element along the diameter, which is similar to the distribution of the ΔC of the Cu element. When conventional DC casting is performed at the casting speed of 65 mm/min, the ΔC of the Mg element is −0.083. The ΔC of the Mg

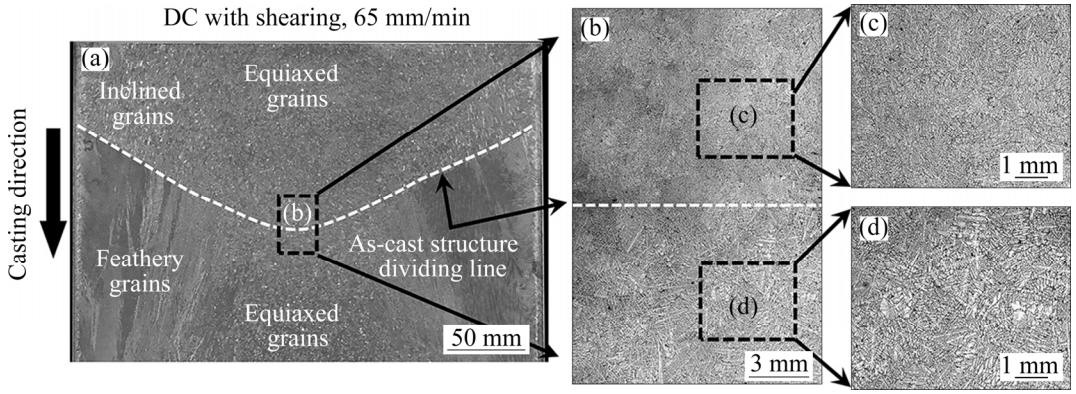

Fig. 9 Transformation of as-cast structure on longitudinal section of ingot: (a) Macrostructure; (b) Microstructure corresponding to dashed rectangular frame in (a); (c, d) Enlarged images of dashed rectangular frame in (b)

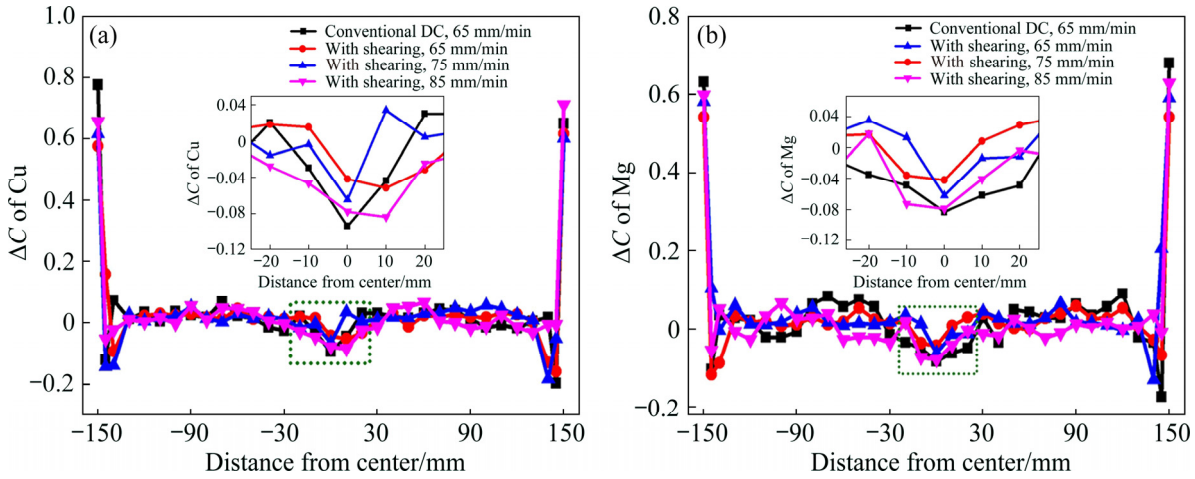

Fig. 10 Cu (a) and Mg (b) segregation patterns in 2024 aluminum alloy ingot under different casting conditions

element decreases to −0.042 after applying the intensive melt shearing. Under the influence of intensive melt shearing, when the casting speed is increased to 75 and 85 mm/min, ΔC values of the Mg element are 0.062 and 0.079, respectively.

4 Discussion

Intensive melt shearing makes the uniform distribution of melt temperature and the cut-down of the superheat of the melt, as shown in Fig. 3. This is mainly because the convection flow generated by the intensive melt shearing can accelerate the heat exchange by transferring the low-temperature melt at the bottom of the sump and near the edge to the center and upper part of the sump. As a result, an approximately isothermal region is formed among the measurement points and the transition region becomes wider. With the increase of casting speed, the high-temperature melt flowing from the launder into the crystallizer increases and the depth of the sump increases, while the cooling capability of the crystallizer and the intensity of the convection flow generated by the intensive melt shearing do not change much (with other parameters unchanged). At the same time, due to the existence of forced convection caused by high-shear unit, the melt temperature at the upper part of the transition region just slightly increases with the increase of casting speed, which is in agreement with the computational simulation of temperature field of DC casting with intensive melt shearing performed by WALINJKAR and RAO [28].

Floating grains are suspended or moved freely in the slurry region until settling down to the solidification interface. There are usually more floating grains in the center of the ingot due to the shape of the sump and the low velocity of the melt flow in the ingot center. Since these grains have a

long residence time in the slurry region and the cooling rate in the slurry region is low, the dendrite arms can sufficiently grow and coarsen. For elements with partition coefficient less than 1 (K<1, such as Cu and Mg), solute atoms are rejected into the liquid melt ahead of the solid−liquid interface and the solid phase becomes depleted during solidification. As a result, the coarse dendrite arms of floating grain are solute-poor. Therefore, the appearance of the floating grains aggravates the negative centerline segregation in the ingot [12]. To further understand the solidification mechanism of the DC casting, schematic diagram of the solidification process is drawn based on the measured temperature curves and the obtained microstructure, as shown in Fig. 11. Because of the relatively wide slurry region (Fig. 11(a)) and relatively low melt flow rate in the center, some grains can be suspended or move freely in the slurry region for a long time [1]. In addition, under the natural convection, the grains move towards the center of the ingot, which is conducive to the increase of the area fraction of the floating grains. After the high-shear unit is inserted and switched on, the heat transfer among the melt, the crystallizer, and the solidified ingot increases on account of the forced convection flow. Consequently, the depth of the sump decreases and the distance between the solidification interface and the tip of the high-shear unit is small (Fig. 11(b)). Moreover, the forced convection flow is concentrated around the tip of the high-shear unit. When the distance from the solidification interface to the tip is short, the collision between the convection flow and the solidification interface is severe, which means that the grains in the slurry region can be quickly transferred to the solidification interface. In the narrow space between the solidification interface and the high-shear unit, these rapidly moving grains are easily captured by the solidification interface and do not have enough time for coarsening, thereby reducing the floating grains and forming fine dendrite arms. As the casting speed increases, the sump depth and the distance between the solidification interface and the high-shear unit increase, though to the less extent as compared to the conventional DC casting. Therefore, when casting speed is high, the intensity of the convection flow in the region near the solidification interface becomes weak. This means that under the convection flow, only a portion of the grains in the slurry region can be quickly transferred to the solidification interface, while the remaining grains circulate around the tip of the high-shear unit, as shown in Fig. 11(c). As a result, the residence time of these grains in the slurry region increases and the dendrite arm becomes coarse, so the area fraction of the floating grains increases when casting speed is increased under the intensive melt shearing. It is suggested that the intensity of the forced convection in the region near the solidification interface plays an important role in the appearance and amount of floating grains. In consequence, to depress the floating grains, the casting speed should be lower or the rotational speed of the rotor should be higher.

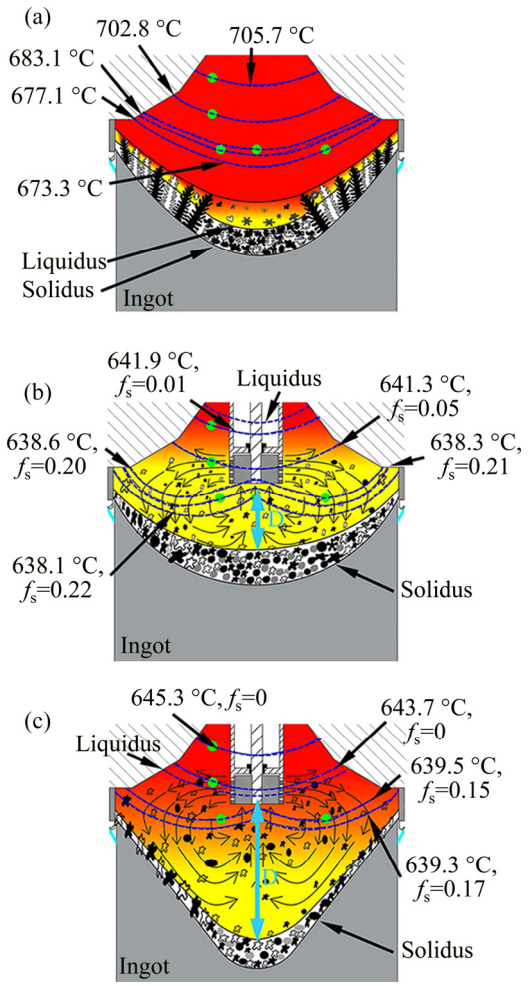

Fig. 11 Schematic diagram of solidification process: (a) Conventional DC, 65 mm/min; (b) With shearing, 65 mm/min; (c) With shearing, 85 mm/min (f_s—Solid fraction)

Shrinkage-induced flow is a melt flow that attempts to compensate for solidification shrinkage, which is perpendicular to the coherence fraction

contour. The horizontal component of this melt flow is from the center of the surface, thus transporting solute from the center to the surface. The deeper and steeper the sump is, the more the solutes will be transported from the center to the surface by the horizontal component of the shrinkage-induced flow [31]. As shown in Fig. 3, the melt temperature decreases rapidly after applying the intensive melt shearing, which means that heat transfer between the melt and the graphite ring, and also between the melt and the solidified ingot increases and contributes to the reduction of the sump. PATEL et al [29] and LOON et al [32] also reported that the depth of the sump could be reduced by applying the intensive melt shearing. Therefore, the intensity of the shrinkage-induced flow is reduced after the intensive melt shearing is applied, which is beneficial to alleviating the negative centerline segregation.

With the application of intensive melt shearing, on one hand, the amount of the floating grains is significantly reduced. On the other hand, the shrinkage flow is decreased due to reduced depth of the sump. In addition, the intensive shearing can generate a convection flow, which flows upward in the center, along the ejection direction in the upper part of the sump, downward at the edge of ingot and correspondingly toward the ingot center along the solidification interface. The forced convection along the solidification interface facilitates the movement of solute-rich melt from the ingot edge to the ingot center and leads to a uniform distribution of solute elements, which helps to alleviate negative centerline segregation. Finally, the negative segregation in ingot center is greatly alleviated under the influence of intensive melt shearing, as shown in Fig. 10. However, as the casting speed increases, sump depth increases [33], resulting in an increase in the intensity of the shrinkage-induced flow. The amount of floating grains in the ingot center also increases. In consequence, the negative centerline segregation becomes more serious with the increase of casting speed under the influence of intensive melt shearing. Besides, the upward centerline forced convections may also affect the negative centerline segregation. However, the role of this upward flow on the negative centerline segregation needs further confirmation.

5 Conclusions

(1) Intensive melt shearing can accelerate the heat transfer, which improves the uniformity of temperature field and decreases the melt temperature in the sump. With the increase of casting speed, the melt temperature increases and the uniformity of the temperature distribution decreases.

(2) At low casting speed, intensive melt shearing can significantly decrease area fraction of the floating grains and distribute them uniformly throughout the ingot, while these effects partially disappear at high casting speed.

(3) Although the centerline segregation could be obviously alleviated by intensive melt shearing, the centerline segregation still becomes increasingly serious with the increase of casting speed under the influence of intensive melt shearing.

Acknowledgments

The authors are grateful for the financial supports from the National Natural Science Foundation of China (51674078, 51374067).

References

[1] GRANDFIELD J F, ESKIN D G, BAINBRIDGE I F. Direct-chill casting of light alloys: Science and technology [M]. Hoboken, New Jersey: John Wiley & Sons, 2013.

[2] ZHU Q F, ZHAO Z H, ZUO Y B, WANG X J, CUI J Z. Effect of low frequency electromagnetic field on as casting structure and surface quality of horizontal direct chill casting 7075 alloy [J]. International Journal of Cast Metals Research, 2013, 25: 93−99.

[3] LIU X, YIN S Q, ZHANG Z Q, LE Q C, XUE J L. Effect of limestone ores on grain refinement of as-cast commercial AZ31 magnesium alloys [J]. Transactions of Nonferrous Metals Society of China, 2018, 28: 1103−1113.

[4] GHONCHEH M H, SHABESTARI S G, ASGARI A, KARIMZADEH M. Nonmechanical criteria proposed for prediction of hot tearing sensitivity in 2024 aluminum alloy [J]. Transactions of Nonferrous Metals Society of China, 2018, 28: 848−857.

[5] ESKIN D G. Physical metallurgy of direct chill casting of aluminum alloys [M]. Boca Raton: CRC Press, 2008.

[6] WANG X J, ZHANG H T, ZUO Y B, ZHAO Z H, ZHU Q F, CUI J Z. Experimental investigation of heat transport and solidification during low frequency electromagnetic hot-top casting of 6063 aluminum alloy [J]. Materials Science and Engineering A, 2008, 497: 416−420.

[7] ZHANG H T, HAN X, WANG D T, SHAO B, QIN K, CUI J Z. Effect of clad ratio on interfacial microstructure and properties of cladding billets via direct-chill casting process [J]. Transactions of Nonferrous Metals Society of China, 2018, 28: 998−1006.

[8] HAN X, SHAO B, ZUO K S, JIANG L, ZHANG H T, HE L Z, QIN K, CUI J Z. Microstructure and properties at bonding interface of AA4045/AA3003 aluminum alloy cladding billet prepared by semi-continuous casting [J]. Transactions of Nonferrous Metals Society of China, 2016, 26: 658−664.

[9] ZUO Y B, CUI J Z, DONG J, XIAO F X. Effects of low frequency electromagnetic field on the as-cast microstructures and mechanical properties of superhigh strength aluminum alloy [J]. Materials Science and Engineering A, 2005: 408: 176−181.

[10] NADELLA R, ESKIN D G, DU Q, KATGERMAN L. Macrosegregation in direct-chill casting of aluminium alloys [J]. Progress in Materials Science, 2008, 53: 421−480.

[11] LUO T J, JI H M, CUI J Z, ZHAO F Z, FENG X H, LI Y J, YANG Y S. As-cast structure and tensile properties of AZ80 magnesium alloy DC cast with low-voltage pulsed magnetic field [J]. Transactions of Nonferrous Metals Society of China, 2015, 25: 2165−2171.

[12] ESKIN D G, NADELLA R, KATGERMAN L. Effect of different grain structures on centerline macrosegregation during direct-chill casting [J]. Acta Materialia, 2008, 56: 1358−1365.

[13] WANG F Y, WANG X J, SUN W, YU F, CUI J Z. Low frequency electromagnetic casting of 2195 aluminum−lithium alloy and its effects on microstructure and mechanical properties [J]. Acta Metallurgica Sinica (English Letters), 2020, 33: 338−350.

[14] LUO H J, JIE W Q, GAO Z M, ZHENG Y J. Numerical simulation for macrosegregation in direct-chill casting of 2024 aluminum alloy with an extended continuum mixture model [J]. Transactions of Nonferrous Metals Society of China, 2018, 28: 1007−1015.

[15] ZHANG L, ESKIN D G, MIROUX A, SUBROTO T, KATGERMAN L. Influence of melt feeding scheme and casting parameters during direct-chill casting on microstructure of an AA7050 billet [J]. Metallurgical and Materials Transactions B, 2012, 43: 1565−1573.

[16] BARBOSA J, PUGA H. Ultrasonic melt processing in the low pressure investment casting of Al alloys [J]. Journal of Materials Processing Technology, 2017, 244: 150−156.

[17] ZUO Y B, CUI J Z, MOU D, ZHU Q F, WANG X J, LI L. Effect of electromagnetic field on microstructure and macrosegregation of flat ingot of 2524 aluminium alloy [J]. Transactions of Nonferrous Metals Society of China, 2014, 24: 2408−2413.

[18] PENG G S, SONG G S, WANG Y, CHEN K H, CHEN S Y. Intensive melt shearing and calcium concentration effects on grain refinement of commercial purity Mg [J]. International Journal of Cast Metals Research, 2017, 31: 99−107.

[19] NADELLA R, ESKIN D G, KATGERMAN L. Effect of grain refinement on structure evolution, “floating” grains, and centerline macrosegregation in direct-chill cast AA2024 alloy billets [J]. Metallurgical and Materials Transactions A, 2008, 39: 450−461.

[20] ESKIN D G, SAVRAN V I, KATGERMAN L. Effects of melt temperature and casting speed on the structure and defect formation during direct-chill casting of an Al−Cu alloy [J]. Metallurgical and Materials Transactions A, 2004, 36: 1965−1976.

[21] ZHU Q F, ZHAO Z H, WANG X J, CUI J Z. The effect of casting speed on sump shape and ingot surface of HDC casting 7075 aluminum alloy ingot [J]. Advances in Materials Research, 2011, 189−193: 3785−3788.

[22] ESKIN D G, DU Q, KATGERMAN L. Scale rules for macrosegregation during direct-chill casting of aluminum alloys [J]. Metallurgical and Materials Transactions A, 2008, 39: 1206−1212.

[23] FAN Z, ZUO Y B, JIANG B. A new technology for treating liquid metals with intensive melt shearing [J]. Materials Science Forum, 2011, 690: 141−144.

[24] YANG X, BAREKAR N S, JI S X, DHINDAW B K, FAN Z. Influence of reinforcing particle distribution on the casting characteristics of Al−SiC_p composites [J]. Journal of Materials Processing Technology, 2020, 279: 116580.

[25] LI H T, ZHAO P, YANG R D, PATEL J B, CHEN X F, FAN Z. Grain refinement and improvement of solidification defects in direct-chill cast billets of A4032 alloy by melt conditioning [J]. Metallurgical and Materials Transactions B, 2017, 48: 2481−2492.

[26] ZUO Y B, JIANG B, FAN Z. Microstructures of DC cast light alloys under the influence of intensive melt shearing [J]. Materials Science Forum, 2011, 690: 137−140.

[27] LIU X D, ZHU Q F, KANG Y L, ZUO Y B, WANG R, LI Z M. An investigation of direct-chill cast 2024 aluminum alloy under the influence of high shearing with regards to different shear positions [J]. Journal of Materials Processing Technology, 2020, 279: 116547.

[28] WALINJKAR D, RAO A K P. C-DC and MC-DC casting of Al-alloys—A comsol approach [J]. Materials Letters, 2015, 161: 698−700.

[29] PATEL J B, LI H T, XIA M X, JONES S, KUMAR S, O'REILLY K, FAN Z. Melt conditioned direct chill casting (MC-DC) process for production of high quality aluminium alloy billets [J]. Materials Science Forum, 2014, 794−796: 149−154.

[30] LIU X D, ZHU Q F, ZUO Y B, ZHU C, ZHAO Z H, CUI J Z. Effect of the intensity of melt shearing on the as cast structure of direct chill cast 2024 aluminum alloy [J]. Metallurgical and Materials Transactions A, 2019, 50: 5727−5733.

[31] ESKIN D G, DU Q, KATGERMAN L. Relationship between shrinkage-induced macrosegregation and the sump profile upon direct-chill casting [J]. Scripta Materialia, 2006, 55: 715−718.

[32] LOON L W, REDDY S S, RAO A K P. CFD simulation of direct chill casting process of magnesium alloy billets [J]. Journal of Manufacturing Processes, 2019, 45: 447−454.

[33] ESKIN D G, ZUIDEMA J, SAVRAN V I, KATGERMAN L. Structure formation and macrosegregation under different process conditions during DC casting [J]. Materials Science and Engineering A, 2004, 384: 232−244.

熔体强剪切作用下铸造速度对半连续铸造2024铝合金铸锭中浮游晶和宏观偏析的影响

刘旭东[1,2]，朱庆丰[1,2]，李志猛[1,2]，朱 成[1,2]，
王 睿[1,2]，贾 涛[2,3]，赵志浩[2]，崔建忠[1,2]，左玉波[1,2]

1. 东北大学 材料电磁过程研究教育部重点实验室，沈阳 110004；
2. 东北大学 材料科学与工程学院，沈阳 110004；
3. 东北大学 轧制技术及连轧自动化国家重点实验室，沈阳 110004

摘 要：在熔体强剪切作用下，采用不同铸造速度的半连续铸造工艺制备铸锭，研究熔体强剪切和其作用下铸造速度对浮游晶和铸锭中心负偏析的影响。结果表明，在半连续铸造过程中施加熔体强剪切可以均匀分布铸锭截面上的浮游晶，减少浮游晶的面积百分数，减弱铸锭中心负偏析，并提高熔池内熔体温度分布的均匀性。在熔体强剪切作用下的半连续铸造过程中，铸造速度对浮游晶的数量和分布起着关键作用。当铸造速度较低时，施加熔体强剪切可以显著减小浮游晶的面积分数，并使其在铸锭内均匀分布。但是，随着铸造速度的增加，这种作用效果逐渐消失。

关键词：半连续铸造；熔体强剪切；宏观偏析；浮游晶；铸造速度；2024铝合金

(Edited by Bing YANG)